Ground-Based Microwave Radiometric Observations of the Temporal Variation of Atmospheric Geopotential Height and Thickness

PIERO CIOTTI, ED R. WESTWATER, MARTIN T. DECKER, MEMBER, IEEE, ALFRED J. BEDARD, JR, AND B. BOBA STANKOV

Abstract—**Since 1981, the Wave Propagation Laboratory of NOAA has operated a ground-based zenith-viewing microwave radiometer. This radiometer, designed to measure precipitable water vapor, cloud liquid, and temperature profiles, has two moisture-sensing channels and four temperature-sounding channels. Data from this system, taken at Denver, Colorado, are used to derive geopotential heights and thicknesses from the surface (about 830 mbar) to 300 mbar. Time series and spectra of several directly measured and inferred quantities are analyzed for different meteorological situations: a period of unusual calm in surface pressure, a frontal passage, and a gravity wave event. The three cases presented illustrate how rapid variations in meteorological variables can be studied using ground-based radiometers. These radiometers provide temporal continuity not hitherto available. The performance of the radiometer, both in observing a blackbody target and during an unusually calm pressure event, shows high sensitivity to changes in geopotential height and thickness and to integrated water vapor. Consequently, the combination of high temporal resolution and high sensitivity allows unique monitoring of rapidly changing conditions, such as frontal passages and gravity wave events. Comparisons of these data with various sources of ground truth, including radiosondes, satellite cloud observations, and arrays of microbarographs, show excellent agreement.**

I. INTRODUCTION

STUDIES have shown that ground-based radiometers can indicate the presence of atmospheric waves [1]–[3]. Spectral analysis of downwelling infrared radiance showed sharp spectral peaks that were associated with waves in the nocturnal boundary layer [1]. Microwave observations also showed peaks that were associated with oscillations of water-vapor density and temperature [2], [3]. The periods of these disturbances are of the order of a few minutes. It would be of practical benefit to observe such oscillations routinely and to interpret them in terms of atmospheric stability, waves, and turbulence.

The ability of a dual-channel microwave radiometer to provide nearly continuous observations of atmospheric precipitable water vapor was shown in [4], [5]. Time series of these data, recorded as 2-min averages, showed rapid moisture variations that would be difficult, if not impossible, to measure by conventional meteorological instrumentation. Spectra of such data showed measurable power up to the 15-cycles/h Nyquist frequency [6]. Since these original observations were made, the radiometric system has been expanded to include four channels in the 60-GHz emission band of molecular oxygen [7]. The complete observing system also includes surface meteorological measurements. The system, except for minor interruptions, has run continuously since 1981 at Stapleton International Airport, Denver, Colorado. Twenty-minute averages of derived temperature and moisture parameters are sent in real time to local users. An archive of 2-min radiometric data is also maintained.

An accuracy analysis of radiometrically derived temperature profiles, based on 20-min averaged data and using colocated National Weather Service (NWS) radiosonde observations (RAOB's) as ground truth, showed rms differences of less than 2°C up to about 500 mbar above the surface [8]. Although the profiles lack high vertical resolution, geopotential heights, derived by integrating these profiles, have an accuracy in the lowest half of the atmosphere comparable to that of RAOB's. Thus, this instrument is capable of providing highly accurate measurements of the short-term behavior of several meteorological parameters. To illustrate this capability, we present 2-min observations of precipitable water vapor, geopotential heights and thicknesses that were taken during three different meteorological situations: a period during which the surface pressure showed a small variance about a near-zero tendency, the passage of a cold front, and a gravity wave event. These observations illustrate how rapid variations in meteorological variables can be studied using ground-based radiometers. By providing a temporal continuity not hitherto available, the high sensitivity of these instruments allows unique monitoring of rapidly changing events.

II. DESCRIPTION OF EQUIPMENT

The radiometer is a component of a ground-based observing system designed to measure profiles of tempera-

Manuscript received August 20, 1986; revised March 24, 1987. A. J. Bedard, Jr. was supported in part by the FAA under contract DTFA01-84-Z-00207.

P. Ciotti is with the Dipartimento di Elettronica, Universitá di Roma La Sapienza, Rome, Italy.

E. R. Westwater, A. J. Bedard, Jr., and B. B. Stankov are with the NOAA/ERL, Wave Propagation Laboratory, Boulder, CO 80303.

M. T. Decker is with the Cooperative Institute for Research in Environmental Sciences (CIRES), University of Colorado, Boulder, CO 80309.

IEEE Log Number 8715876.

ture and wind, as well as integrated amounts of precipitable water vapor and cloud liquid. Instrumental details of the system are described in [7]. Here, we describe only the radiometric portion of the system. The radiometric system is located less than 50 m from the NWS RAOB launch site. The six-channel radiometer has one channel operating at 20.6 GHz, one at 31.65 GHz, and channels at 52.85, 53.85, 55.45, and 58.8 GHz. All channels of the zenith-viewing system have equal beamwidths of 2.3 degrees. The lower two channels are sensitive to water vapor and cloud liquid; the weak absorption at these frequencies allows calibration by the "tipping curve" method [5]. The upper four channels are most sensitive to temperature. Their calibration requires comparison of clear-sky measurements with calculations of brightness temperature (T_b) from height profiles of temperature, absolute humidity, and pressure measured by RAOB's. The absolute accuracy of the channels is discussed in Section IV.

The emission measurements are supplemented with surface observations of temperature T_S, pressure P_S, and relative humidity $(RH)_S$. Two-minute averages of all nine observations are sampled every 2 min. For approximately 6 min at the start of every hour, an internal calibration cycle is performed. Thus, for every hour, a total of 27 nine-component data vectors are recorded and archived, and three data points are missing.

III. Methodology

A. Retrieval Method

We derive vertical profiles of temperature and humidity from sky brightness observations by linear *a priori* statistical inversion [8]. With this technique, a profile is estimated from a linear combination of the components of the measured data vector; the coefficients used in this combination are determined by minimizing, over a suitably chosen ensemble, the expected mean square error between a profile and its estimate. Let y be a vertical coordinate (such as height) and y_i, $i = 1, 2, \cdots, m$, be a suitably dense set of discrete values of y. We represent a vertical profile of a parameter $p(y)$ by an m-dimensional vector $\boldsymbol{p} = (p(y_1), p(y_2), \cdots, p(y_m))^T$; similarly, n separate components of data are represented by an n-dimensional column vector $\boldsymbol{d}$. Our particular data vector consists of optical depth derived from brightness temperatures (2 components), brightness temperatures (4 components), and surface meteorological observations (3 components). We derive $\boldsymbol{p}$ by a minimum variance unbiased estimator $\hat{\boldsymbol{p}}$ given by

$$\hat{\boldsymbol{p}} = \langle \boldsymbol{p} \rangle + \langle \boldsymbol{p}'\boldsymbol{d}'^T \rangle \langle \boldsymbol{d}'\boldsymbol{d}'^T \rangle^{-1} (\boldsymbol{d} - \langle \boldsymbol{d} \rangle) \quad (1)$$

where $\langle\ \rangle$ represents ensemble averaging over a joint distribution of profiles and data, v^T is the transpose of the vector v, and the primes refer to departures from ensemble averages, e.g., $v' = v - \langle v \rangle$. Application of (1) requires knowledge of 1) the mean vectors ($\langle \boldsymbol{p} \rangle$, $\langle \boldsymbol{d} \rangle$); 2) the cross-covariance matrix between profiles and data ($\langle \boldsymbol{p}'\boldsymbol{d}'^T \rangle$), and 3) the covariance matrix describing the noise degraded data ($\langle \boldsymbol{d}'\boldsymbol{d}'^T \rangle$).

For our ground-based radiometric application, an extensive set of both profiles and brightness temperature observations was not available. However, given that our equipment noise levels are known, and that microwave brightness temperatures can be accurately calculated from RAOB's [8], we relied on a past history of RAOB's to calculate the required statistical quantities in (1). In particular, the ensembles we used to compute retrieval coefficents from (1) were selected from NWS RAOB's taken at Denver, Colorado, during 1972–1977. For the ith month ($i = 1, 2, \cdots, 12$), coefficients were computed from data representing the months $(i - 1)$, i, and $(i + 1)$. Clouds were simulated using models [9], and radiometric noise levels were determined experimentally as described in Section IV.

The geopotential height $h(P)$ in meters at pressure P in millibars is related to the virtual temperature profile $T_V(P)$ in degrees Kelvin by

$$h(P) = -(R/g) \int_{\ln P_S}^{\ln P} T_V(P)\, d \ln P \quad (2)$$

where P_S is the surface pressure, R is the gas constant for dry air, and g is the acceleration of gravity. For $h(P)$ in geopotential meters, $R/g = 29.29$. The geopolitical thickness between two pressure levels P_1 and P_2 is given by

$$t(P_1, P_2) = h(P_2) - h(P_1) = -(R/g) \int_{\ln P_1}^{\ln P_2} T_V(P)\, d \ln P. \quad (3)$$

Alternatively, (3) can be related to an average virtual temperature $T_v^*(P_1, P_2)$ by

$$T_v^*(P_1, P_2) = (g/R)\, t(P_1, P_2)/\ln (P_1/P_2). \quad (4)$$

Since $h(P)$ and $t(P_1, P_2)$ are linear measures of the $T_V(P)$ values, and since $T_V(P)$ is approximately linearly related to the actual temperature and absolute humidity, we greatly simplified the retrieval procedure by directly estimating $h(P)$ at 100-mbar increments from 800 to 300 mbar. In a few cases, we checked this approximation by inserting the radiometrically derived temperature and humidity profiles in (2), and compared the results with the directly estimated quantities. In these cases, the heights agreed to within 1 m.

B. Method for Inserting Missing Data

As discussed in Section II, each hour of data consists of equally spaced 2-min samples (sampling frequency is 30 cycles/h) of 2-min averages, with three missing data samples at the start of each hour. To compute spectra from the data over time intervals greater than 54 min, a scheme to insert the three missing 2-min averages was necessary. Let d_i, $i = 1, 2, \cdots, 9$ be consecutive data three points before, three points during, and three points after calibra-

tion time. The data d_4, d_5, and d_6 are missing. In terms of the quantity $\delta_{i,j} = d_i - d_j$, we computed the missing points by

$$\hat{d}_4 = d_3 - 0.5\delta_{2,3}$$
$$\hat{d}_5 = [(d_3 - 0.3\delta_{1,3}) + (d_7 + 0.3\delta_{7,9})]/2$$
$$\hat{d}_6 = d_7 + 0.5\delta_{7,8}. \quad (5)$$

This scheme is illustrated in Fig. 1. Tests of the method were made using time series of uncorrelated Gaussian noise. We observed only negligible differences between spectra calculated from the original and from the interpolated time series.

C. Spectral Analysis

In the following sections, we present radiometric data that were obtained when gravity wave activity was known independently to be occurring. In general, our measured brightness temperatures are influenced by "white" noise of the radiometer's receiver, by turbulent fluctuations of temperature and water vapor, and by coherent oscillations of waves. The spectra of atmospheric turbulent fluctuations are frequently characterized by a "$-5/3$" law. Thus, to analyze such complex data, some care is needed in choosing both a spectral analysis method and the parameters associated with the method. We selected two types of spectral analysis procedures to apply to radiometrically derived quantities. The first was conventional discrete Fourier transform analysis (FT); the second, the autoregressive spectral method (AR). Our computer codes used routines from the National Bureau of Standards Statistical Library (STARPAC) that were coded following [10]. For completeness, we will outline below a short description of the two methods.

We assume that we have a digital time series obtained by sampling a finite length realization of a stationary random process $x(t)$, $-\infty \leqslant t \leqslant \infty$. The random process is characterized by a spectral density $C_{xx}(f)$ as a function of frequency f. The function $C_{xx}(f)$ is theoretically equal to the Fourier transform of the autocovariance function $c_{xx}(\tau)$, where

$$c_{xx}(\tau) = \langle (x(t) - \langle x \rangle)(x(t+\tau) - \langle x \rangle) \rangle. \quad (6)$$

In (6), $\langle x \rangle$ is the ensemble average of $x(t)$, τ is the temporal lag, and the expectation operation is taken over an ensemble of realizations of $x(t)$. Assuming that time averages are equivalent to ensemble averages, from a single realization of $x(t)$, the FT method estimates the spectral density as the Fourier transform of the sample autocovariance function. However, as is clearly discussed in [10], [11], smoothing (or averaging) in the frequency domain is necessary to reduce statistical variance of the estimate. Furthermore, as the variance is reduced by smoothing, the bias is increased. A reasonable compromise between bias and variance is required to achieve a meaningful estimate. The required smoothing can be achieved by operations either in the frequency domain or in the time domain.

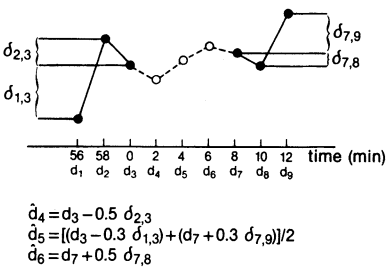

Fig. 1. Schematic drawing of the method used to insert missing data.

From a digital time series of x_i, $i = 1, 2, \cdots, N$, with a sampling period of Δ, the FT algorithm computes a smoothed spectrum estimator $\bar{C}_{xx}(f)$ as

$$\bar{C}_{xx}(f) = 2\Delta\left\{c_{xx}(0) + 2\sum_{k=1}^{N-1} c_{xx}(k)\, w(k) \cdot \cos(2\pi k f \Delta)\right\}, \quad 0 \leqslant f \leqslant \frac{1}{2\Delta}. \quad (6)$$

The sample autocovariance function $c_{xx}(k)$ is

$$c_{xx}(k) = \frac{1}{N}\sum_{i=1}^{N-k} (x_i - \bar{x})(x_{i+k} - \bar{x}), \quad 0 \leqslant k \leqslant N-1. \quad (7)$$

In (6) and (7), $\bar{x}$ is the sample average of x_i, k is the lag, and the weighting function $w(k)$ is called the lag window. A discussion of several choices of $w(k)$ is given in [10] and [11]. The Fourier transform of the lag window is called the spectral window $W(f)$. Various numerical factors have been adjusted in (6) to preserve the Fourier transform relationship between the sample spectrum and the sample autocovariance function. Usually, for a given lag window, a maximum lag M, called the lag truncation point, is chosen. In terms of the sampling period Δ, the length of the lag window is $M\Delta$.

We chose for our FT analysis the Parzen window W_P [10], [11] because: 1) it yields a spectral estimate with small variance, 2) it is strictly positive, and 3) it decays smoothly with frequency. In the frequency domain, the form of $W_p(f)$ is

$$W_P(f) = \frac{3}{4} M\Delta\left(\frac{\sin(\pi f M\Delta/2)}{\pi f M\Delta/2}\right)^4. \quad (8)$$

The bandwidth, variance ratio, and degrees of freedom associated with $W_P(f)$ are discussed in [10]. In particular, the (relatively large) bandwidth is $1.86/M\Delta$. For all of the data sets we spectrally analyzed (see Sections IV–VIII), various choices of M were investigated. For the time series of approximately 2-h length, a choice of $M\Delta$ = (record length)/4 gave good stability and yet picked out spectral peaks.

In contrast to FT methods, which employ smoothing by means of a suitable spectral window, autoregressive methods estimate the parameters of an AR model from the data, and then substitute those values in the theoretical expression for the spectral density function [11]. To use

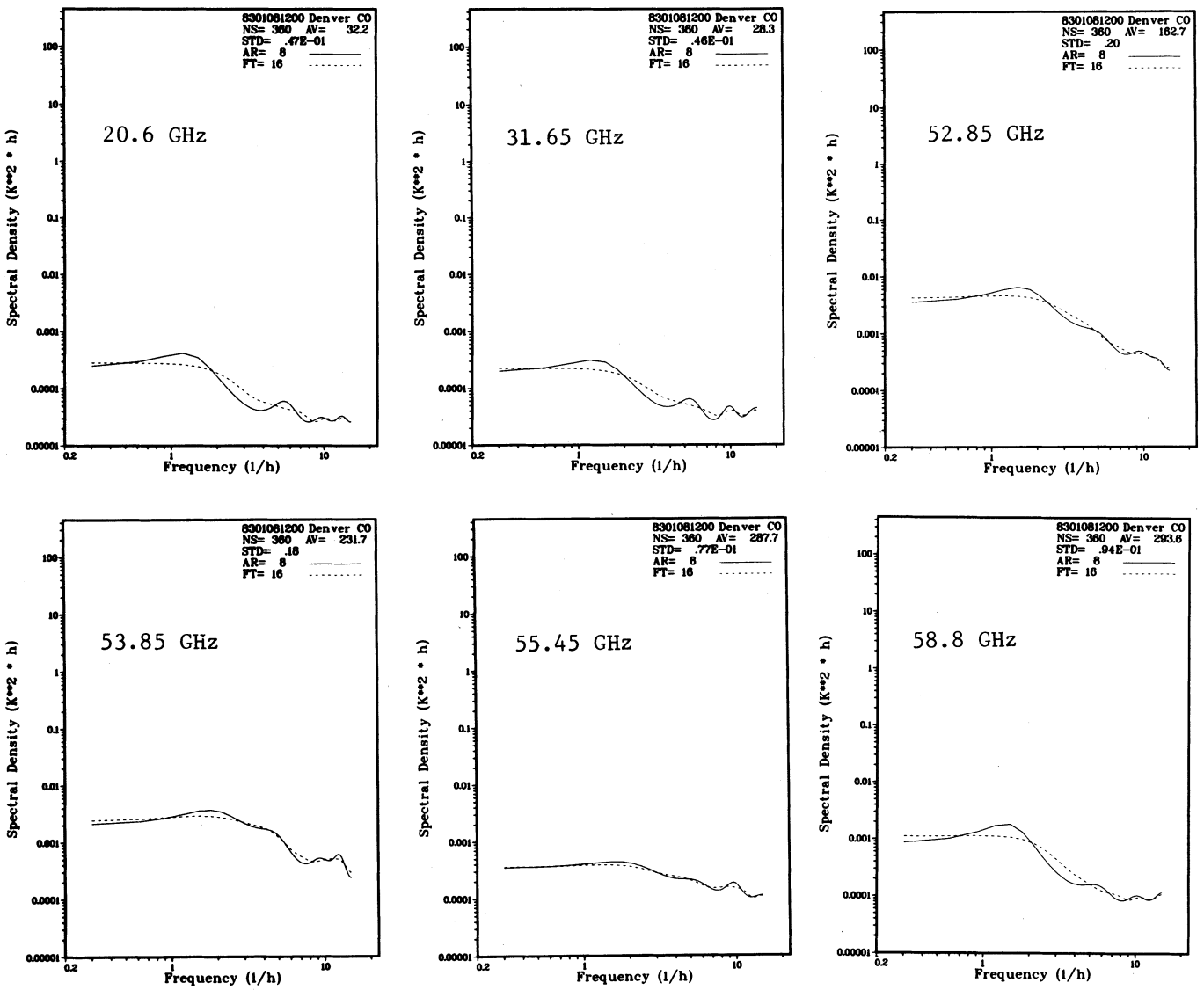

Fig. 2. Spectral density of brightness temperatures obtained with the radiometer's antennas viewing a blackbody target. Spectral densities of all figures are normalized such that their integrals are equal to one half of the total variance. *AR*, the order of autogressive spectrum, is 8; *FT*, the maximum lag of Fourier spectral method, is 16; record length is 12 h; *NS* is the sample size of 360.

this method, the order m of the AR model must be specified. The uncertainty in the choice of m corresponds roughly to the choosing M for the FT method. Again, by trial and error and by comparing results with the FT method, we chose $m = M/2$.

IV. Noise and Accuracy

In subsequent portions of this paper, we report on observations based on the temporal and spectral variation of atmospheric thermal emission. To establish a baseline value against which atmospheric variations could be compared, T_b's were measured with the radiometer's antennas pointing at a blackbody target that was located on the ground outside the radiometer's equipment trailer. From a 12-h segment of detrended data, we derived 1) spectra of T_b's at each of the 6 channels, and 2) the 6×6 covariance matrix describing the fluctuation levels. As shown in Fig. 2, the spectra have a broad maximum at about 1 cycle/h and then decrease somewhat with frequency. It is suspected that the peak at 1 cycle/h is connected with small instrument changes that occur during the hourly calibration cycle. However, computer simulations indicated that the peak was not introduced by the method for inserting missing data (see Section III-B). The 2-min rms noise levels are shown in Table I. In addition, this table gives absolute accuracies, estimated from a series of 99 independent comparisons of measurements and brightness temperatures calculated from RAOB's.

Two recent papers [8], [12] evaluated the accuracies of ground- and satellite-based radiometric determinations of $h(P)$ and $t(P_1, P_2)$. These comparisons, based on one year of data with a total sample size N of 460, showed that radiometric accuracies of heights and thicknesses were achieving parity with those of conventional RAOB's. As a convenient reference, we show in Table II various measures of $h(P)$ accuracy that are relevant here. In interpreting the numbers given in this table, we note that at Denver, Colorado, the location at which the measure-

TABLE I
ACCURACY OF THE SIX-CHANNEL RADIOMETER

Frequency (GHz)	Estimated absolute error (K)	2-min rms fluctuations (K)
20.60	1.05	0.047
31.65	0.75	0.046
52.85	0.86	0.200
53.85	0.63	0.187
55.45	0.90	0.077
58.80	0.64	0.094

TABLE II
COMPARISON OF rms ACCURACIES OF GEOPOTENTIAL HEIGHT (m) DETERMINATION
(The equivalent accuracies of layer-averaged virtual temperature (in degrees Celsius) are given in parentheses, using an average surface pressure of 835 mbar.)

Pressure level (mb)	RAOB precision*	RAOB-Profiler	Theoretical accuracy	Noise equivalent geopotential std. deviation
700	5.1(0.99)	3.8(0.74)	3.5(0.68)	0.7(0.14)
500	12.7(0.85)	13.1(0.87)	12.8(0.85)	2.5(0.17)
300	20.3(0.68)	33.0(1.10)	33.8(1.13)	9.1(0.30)

*From Hoehne [13].

ments were taken, P_S ranges from about 850 to 820 mbar. Hoehne's [13] evaluation of RAOB accuracy of $h(P)$ used observations taken at sea level, and we adjusted his values to Denver pressures. In Table II, the theoretical rms accuracies are given. These quantities were calculated by regression analysis using 1) the 1972–1977 data base of Denver NWS RAOB's, 2) the brightness temperatures calculated from these RAOB's, and 3) the rms brightness temperature's errors given in Table I. In addition, rms absolute accuracies of 0.5°C, 0.05, and 0.1 mbar were assumed in surface instrument measurements of T_s, $(RH)_s$, and P_s. We note the close agreement between the theoretical and achieved (RAOB-Profiler) rms accuracies.

As a measure of the influence of radiometric and surface meterological noise on retrieved heights, we show in Table II the noise equivalent geopotential height variations. These quantities were calculated by applying (1) to data vectors formed from the 12-h samples of target and surface instrument noise. The surface meteorological noise (precision, not absolute accuracy) was simulated by Gaussian noise of rms values of 0.1°C, 0.01, and 0.01 mbar for T_s, $(RH)_s$, and P_s.

TABLE III
ACCURACY OF RADIOMETRIC DETERMINATION OF MOISTURE

VAPOR	
rms accuracy (theoretical)	0.7 mm
rms difference from RAOB's	1.7 mm
2-min rms sensitivity	7.3×10^{-2} mm
LIQUID	
rms accuracy (theoretical)	3.3×10^{-2} mm
2-min rms sensitivity	5.2×10^{-3} mm

The derived accuracies and spectra of $h(P)$ are sensitive to the assumed level of surface pressure noise. Roughly speaking, a 1-mbar change in P_s is equivalent to a 10-m change in $h(P)$. Thus, even a 0.1-mbar uncertainty leads to height uncertainty that is an appreciable fraction of the radiometer's height measurement capability. In the same manner, the absolute accuracy and precision of the radiosonde baroswitch limit the accuracy of the radiosonde-derived pressure heights. In Section V, we present a surface pressure spectrum taken during calm pressure conditions that is consistent with our 0.01-mbar assumption.

In addition to the quantities primarily related to temperature, the radiometric Profiler also provides 2-min averages of precipitable water vapor and cloud liquid (the radiometer is not sensitive to cloud ice). For completeness, we summarize in Table III the accuracies and sensitivities of these quantities. As was noted by Hogg *et al.*, [5] RAOB and Profiler measurements of precipitable vapor are of comparable accuracy. As in the case of geopotential height determinations, the sensitivity to moisture changes is roughly an order of magnitude better than the absolute accuracy.

V. CALM CASE

In Sections VI and VII, an analysis is given of observations taken during time-varying meteorological events. As a contrast, and as evidence that our derived noise levels are reasonable, we present here observations taken during calm conditions. On July 11, 1984, a surface array of microbarographs had indicated an unusually low level of pressure fluctuations. To analyze the performance of the radiometer during such conditions, we examined a 30-h segment of data around this time period. A 2-h period was found in which radiometric fluctuations were also low. We show in Fig. 3 the spectra of the T_b values for each channel, surface pressure P_s, surface temperature T_s, and dew point temperature T_d. We also show on the T_b plots the noise spectra that were estimated from the target experiment. Fluctuations in the T_b's for the four higher frequency channels are approaching the noise levels, although slight warming trends were present in the 55.45- and 58.80-GHz channels. During this time, T_S increased about 6°C. However, the fluctuations in the 20.6- and the

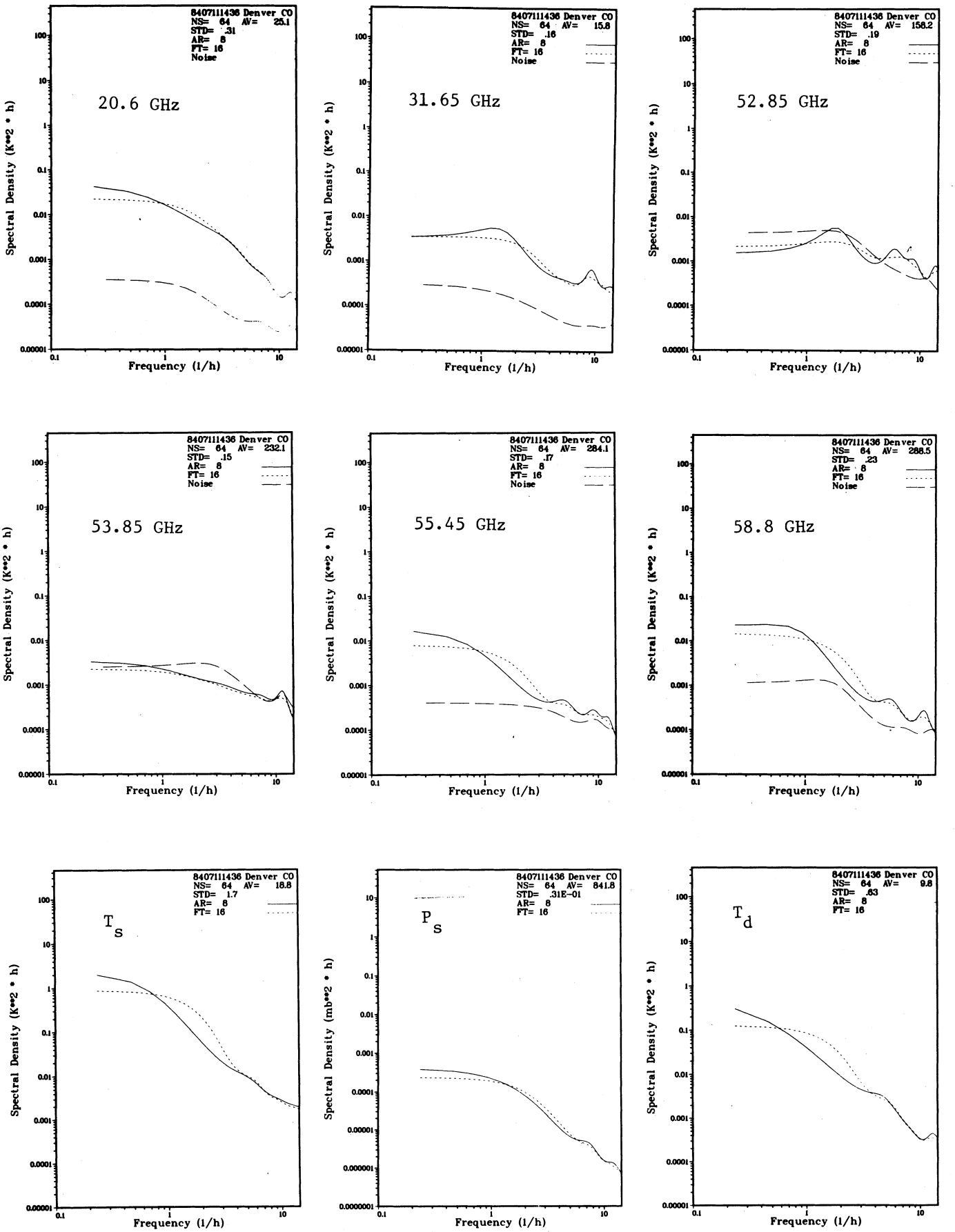

Fig. 3. Calm pressure case, July 11, 1984, 1230–1436 GMT: Spectral density of brightness temperatures and surface observations. Record length is 128 min; $NS = 64$; $AR = 8$; $FT = 16$.

31.65-GHz channels were roughly a factor of 5 higher than the noise. We denote by σ_x the standard deviation of the quantity x. Fluctuations in P_s ($\sigma_p = 3.1 \times 10^{-2}$ mbar) are from 10 to 100 times less than those of the events that we analyze in Sections VI and VII. To demonstrate the impressive precision of microwave radiometers, we show that during the 128 min of the calm case, P_s fluctuations are almost entirely due to precipitable water vapor V. If we derive V from the two moisture channels, a value of $\sigma_v = 2.9 \times 10^{-2}$ cm is obtained. This fluctuation of the total mass of water vapor contributes to the P_s fluctuations an amount 2.8×10^{-2} mbar, or about 90 percent of the total.

From the time series of the measured data vector, a corresponding series of various meteorological quantities was derived. Spectra of these quantities are shown in Fig. 4. We observed that, with the exception of V, the spectra are close to the estimated noise levels.

VI. Passage of a Cold Front

The ground-based radiometer has the ability to monitor important features of rapidly changing meteorological events [14]. We illustrate this capability by presenting observations taken for a 30-h period on December 19–21, 1983, during which a cold front passed over Denver. In Fig. 5 time series are shown of several directly measured and inferred meteorological variables. We focus on the first 18 h of the record. Starting at 1800 GMT on December 19, P_s decreased steadily to a minimum at 1100 GMT on December 20. During this period, the total pressure drop was 11 mbar. Although substantial decreases were occurring in T_s, the layer thicknesses showed a slight increase (warming). From (2), $h(P)$ depends on P_s, which was decreasing, and on the mean $T_V(P)$, which was roughly a constant. Consequently, the decrease in height was basically due to the trend of P_s. After 1200 GMT, the thicknesses decreased substantially, reflecting the arrival of the cold air mass. Precipitable water vapor and cloud liquid are also shown, but no dramatic behavior is evident in these variables. Because of the low temperatures, the observed liquid is probably supercooled. We note that there is no "contamination" of the height and thickness retrievals by either the vapor or the liquid. RAOB determinations of various quantities are also shown in this figure.

Another way of depicting the passage of the cold front is through height contours of potential temperature θ. This quantity is defined by

$$\theta = T(1000/P)^{0.286} \tag{9}$$

where T is the absolute temperature in degrees Kelvin and P is the pressure in millibars. The potential temperature is a conservative quantity during an adiabatic process. The time series of these height contours shown in Fig. 6. again shows the sudden cooling in the atmosphere above 700 mbar that starts around 1100 GMT. Although there is some cooling of the layers below 700 mbar, as evidenced by the increase in height of θ, the larger changes are clearly occurring above this level. Also connected by straight lines in Fig. 6 are the values of θ determined from RAOB's. Although θ is a point quantity, and hence is not inferred as well as a spatially integrated quantity, the agreement with the RAOB determination is generally good.

The three RAOB's from which heights and thicknesses were derived are shown in Fig. 7. We note the sharp frontal temperature inversion whose depth increases temporally as the front undercuts the warmer air aloft. The temperature aloft on December 20 at 2300 GMT is roughly 10°C colder than the previous two soundings. The radiometrically derived thicknesses shown in Fig. 5 agree quantitatively with all three RAOB's. Also, note the high winds in the 500–300 mbar region and the wind directional shift in the vicinity of the elevated temperature inversion at around 700 mbar.

Fig. 5 also shows that the variances of the thicknesses were substantially greater in the period starting approximately 12 h before the time of the pressure minimum. This period was also one of intense wave activity, as was observed independently by a surface-based microbarograph array. We therefore examined various 1 and 2-h segments of the 12-h period for the presence of waves. Typical 128-min spectra of $t(P_1, P_2)$ and P_s are shown in Fig. 8. We note that P_s has two peaks, one at 8.0 cycles/h and another at 12.5 cycles/h. Each of the radiometrically derived thickness spectra has a spectral peak in the vicinity of 7.5 cycles/h, and $t(600, 500$ mbar) also has a peak at 12.0 cycles/h. The bandwidth of the FT spectral estimation (64 2-min samples) is 3.48 cycles/h. Thus, the spectral peaks that are present in P_s (at the radiometer's location) are also present in the thickness. Pressure data from a microbarograph array, located about 30 km NW of the radiometers, yielded spectral peaks at 7.0 and 15.0 cycles/h.

Surface pressure P_s is one of the components of the data vector used to estimate $h(P)$ and $t(P_1, P_2)$. Thus, spectral peaks in P_s could induce corresponding peaks of the derived radiometric spectra. However, the magnitude of the pressure retrieval coefficient for thickness between pressure levels is sufficiently small that negligible contamination will arise from this component. For example, the pressure coefficient for $t(600, 500$ mbar) is 0.7 m/mbar. From the two-sided spectra of Fig. 8, the pressure variance in the 6.5 to 9.5 cycles/h region is 5×10^{-4} mbar^2. If we multiply the square of the coefficient by the pressure variance to yield thickness variance, we get 2.5×10^{-4} m^2, some 3–4 orders of magnitude less than the value of the spectral peak in the derived thickness (~ 1 m^2) shown in Fig. 8. We also performed a numerical experiment to evaluate this effect. We added a pure sine wave of 0.1-mbar amplitude and 10-min period to a 2-h segment of real data and then derived thickness spectra. There was no suggestion of the sinusoid in the derived spectra. Thus, we feel confident that the correspondence of the spectral peaks is indicative of physical processes

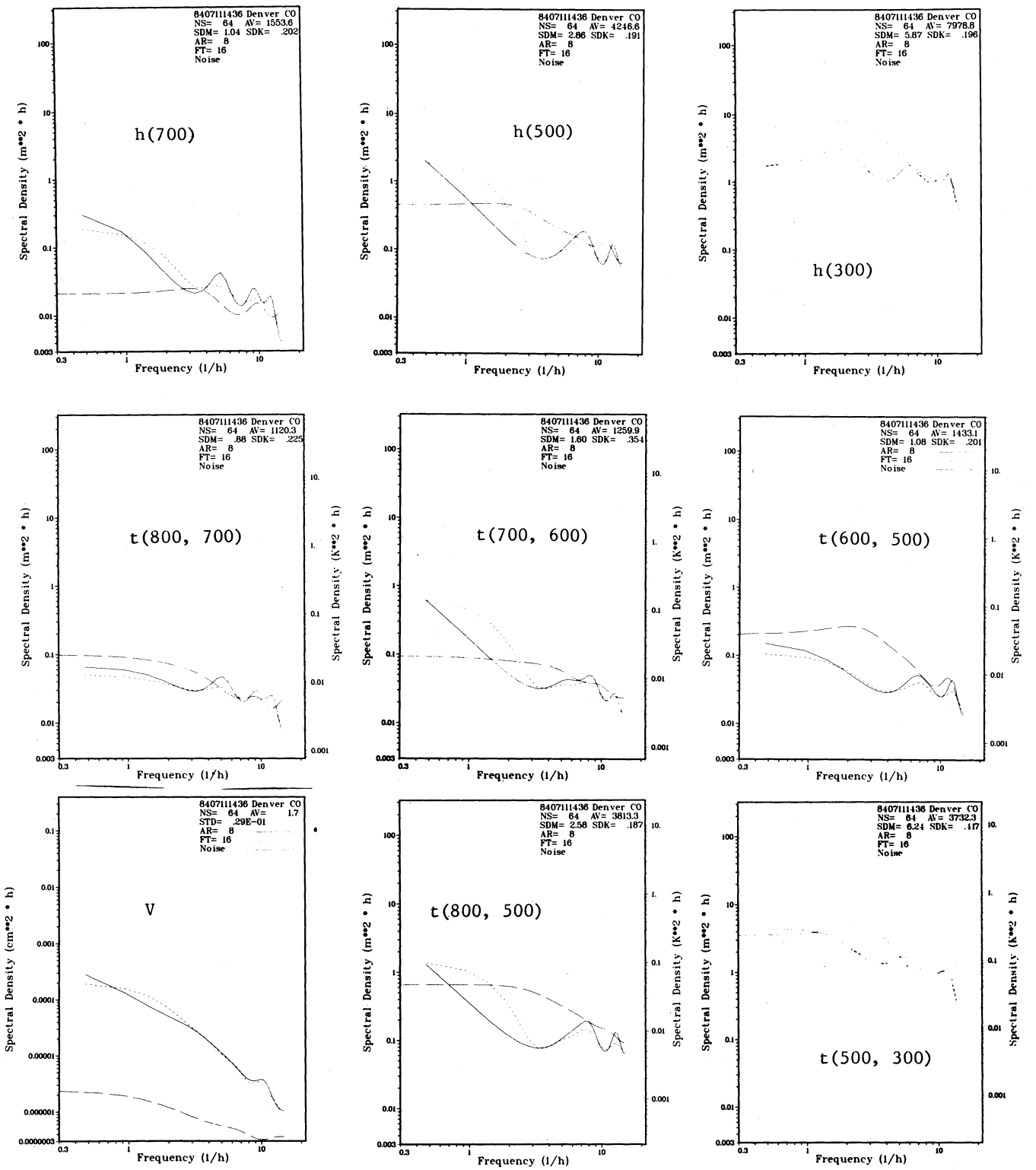

Fig. 4. Calm pressure case, July 11, 1984, 1230–1436 GMT: Spectral densities of derived meteorological parameters. Record length is 128 min; NS = 64; AR = 8; FT = 16.

occurring in the atmosphere and is not an artifact of data processing.

An anonymous referee quite appropriately pointed out that there is a possibility of contamination of the brightness temperature fluctuation data from pressure fluctuations. This occurs physically because of pressure broadening of the absorption lines and the subsequent effect in the atmospheric transmission profile. We can evaluate the magnitude of this effect using linear analysis. A vertical profile of small perturbations in pressure $\delta P(h)$ will give rise to changes in T_b by

$$\delta T_b = \int_0^\infty W_p(h)\, \delta P(h)\, dh \qquad (10)$$

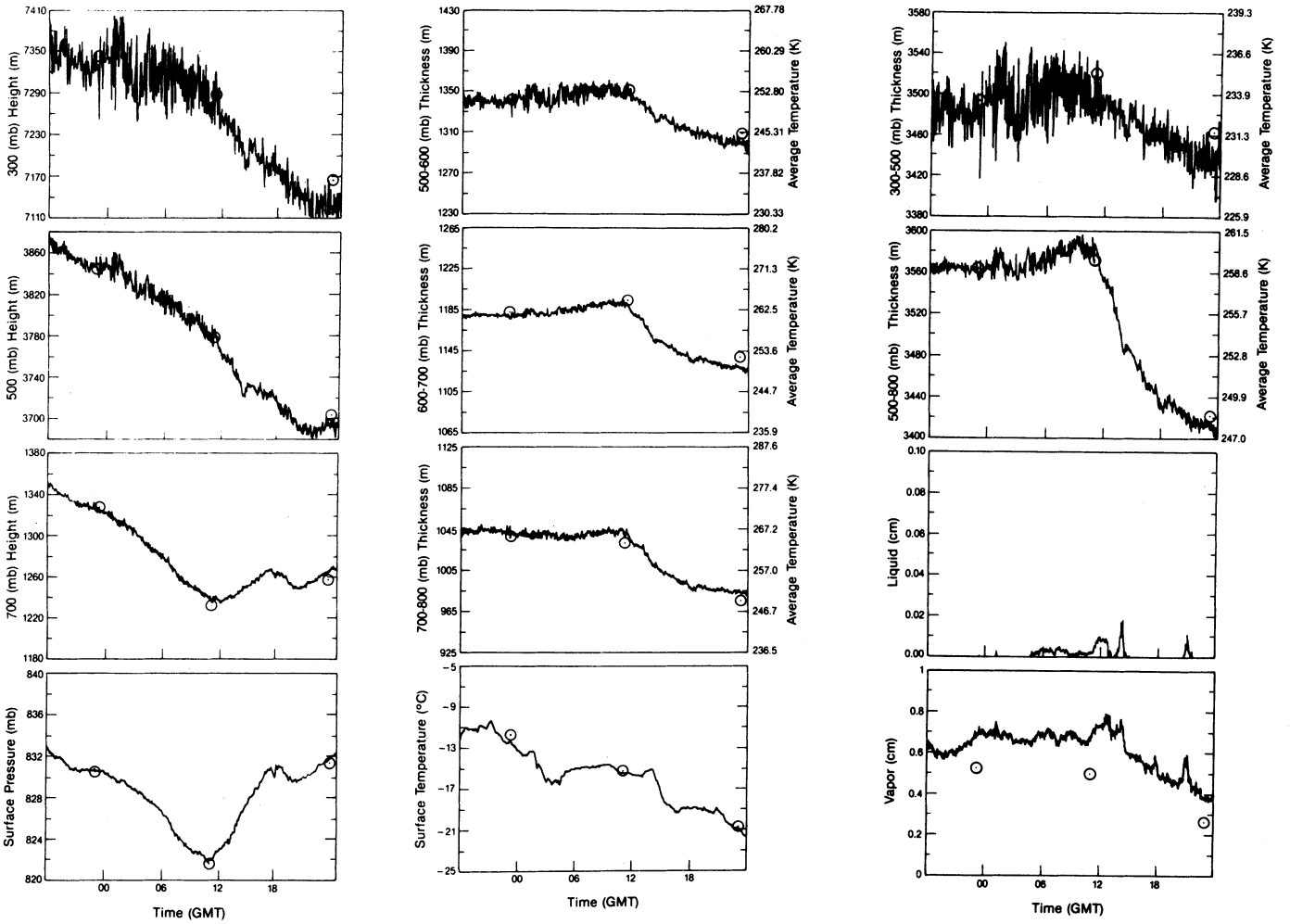

Fig. 5. Cold front, December 19, 1984, 1802 GMT, to December 21, 1984, 0000 GMT: 30-h time series of directly measured and derived meteorological parameters. Circled quantities refer to RAOB measurements.

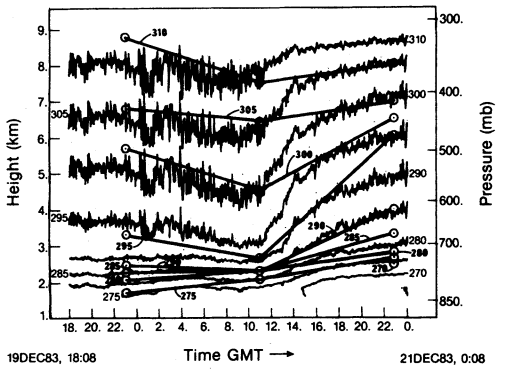

Fig. 6. Cold front, December 19, 1984, 1802 GMT, to December 21, 1984, 0000 GMT: 30-h time series of potential temperature contours. Because of the variation of surface pressure during this event, the pressure ordinate is only approximate. Circled quantities refer to RAOB measurements.

where the pressure weighted functions $W_p(h)$ can be calculated from a perturbation analysis of the radiative transfer equation [15]. The pressure weighting functions for the six-channel profiler are shown in Fig. 9. It is evident from this figure that the 52.85 GHz (C3) and the 53.85 GHz (C4) channels are the principal candidates for influence by pressure fluctuations. We will estimate the magnitude of this effect for the two channels. Fig. 9 shows that the (C3, C4) weighting functions are approximately exponentially distributed with scale heights H_W of 9 and 10 km, respectively. We assume, then, that

$$W_p(h) \approx W_p(0)\, e^{-h/H_w} \tag{11}$$

and, also, that

$$\delta P(h) \approx \delta P(0)\, e^{-h/H_p} \tag{12}$$

where we choose a nominal value for the pressure scale height H_p to be 7.5 km. Inserting (11) and (12) into (10) and integrating leads to

$$\delta T_b \approx W_p(0)\, H_c\, \delta P(0) \tag{13}$$

where

$$\frac{1}{H_c} = \frac{1}{H_w} + \frac{1}{H_p}.$$

From the assumed scale heights and the weighting functions at the surface, we estimate

$$\delta T_b = 0.21 \delta P(0) \text{ for C3}$$

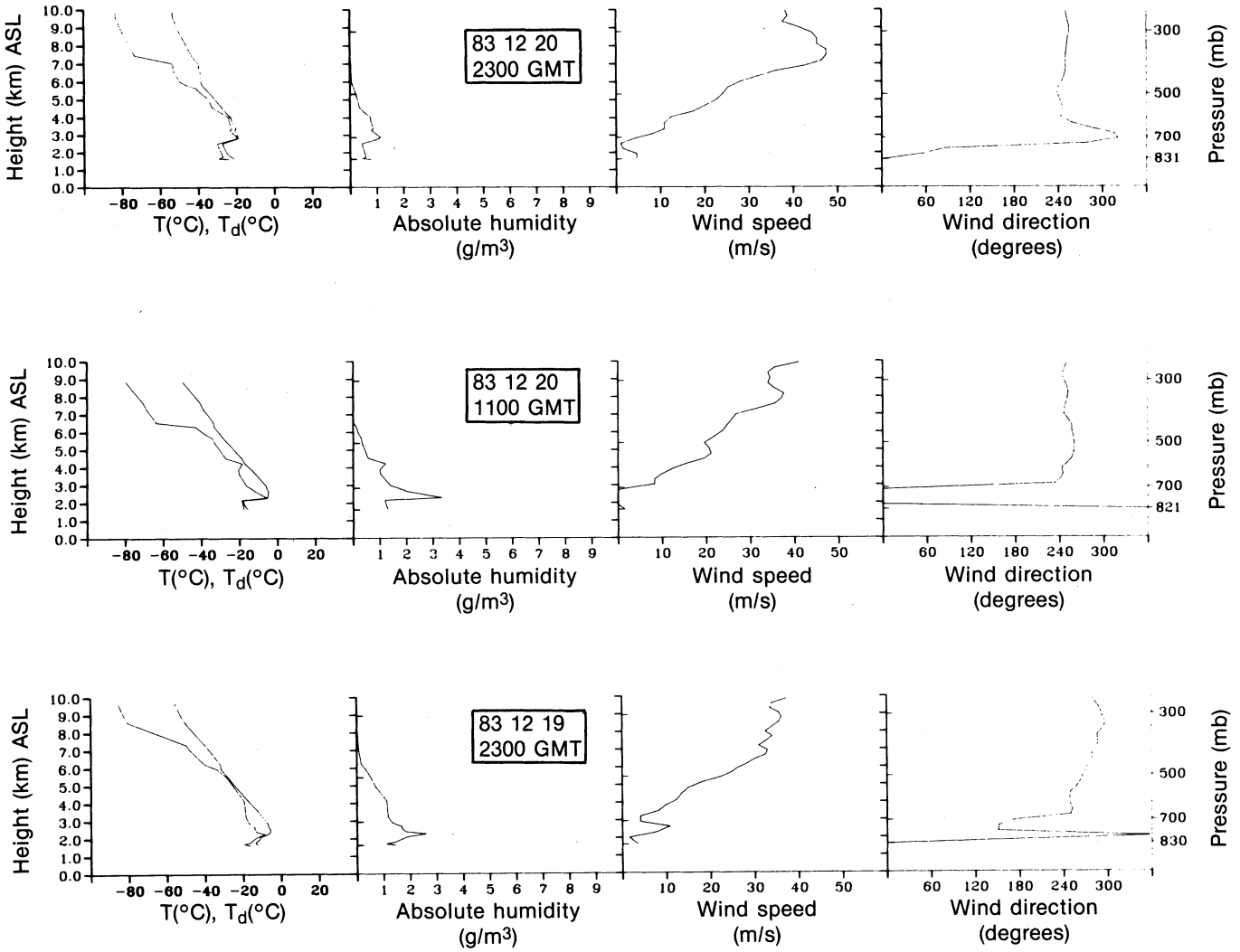

Fig. 7. Cold front, December 19-21, 1983: NWS RAOB's.

and

$$\delta T_b = 0.15\delta P(0) \text{ for C4.}$$

Now, for pressure changes of ~ 1 mbar, the resultant δT_b's would be of the order of the noise levels shown in Table I, and a contamination would result. However, even for a relatively large perturbation amplitude of 0.1 mbar, the resulting T_b changes are about a factor of 10 below the noise. For example, the pressure perturbation amplitudes (relative to the normal background pressure decay with frequency) for the spectral peak at ~ 8 cycles/h in Fig. 8 and at ~ 6 cycles/h in Fig. 12 both have amplitudes of the order of 0.02 mbar. Thus, for the cases presented in Sections VI and VII, and for the relatively high noise levels of the 52.85- and 53.85-GHz channels, pressure-induced fluctuations in transmission did not contribute significantly to the spectra.

For a more sensitive radiometer, noise levels could be reduced by an order of magnitude. For these instruments, transmission fluctuations due to large pressure fluctuations could conceivably contribute to spectra. However, even in this case, nearly uncontaminated spectra of geopotential thicknesses could be constructed by using a modified brightness temperature variable, e.g.,

$$T_b \rightarrow T_b - W_p(0)\, H_w\, \delta P(0)$$

or

$$T_b \rightarrow T_b - \langle T_b' P_s' \rangle \langle P_s'^2 \rangle^{-1} \left(P_s - \langle P_s \rangle\right).$$

VII. Observations During a Gravity Wave Event

During February 2-4, 1984, observations from several different sensors indicated the presence of gravity wave activity occurring in the middle troposphere. These sensors included a surface array of microbarographs, time sequences of satellite cloud photographs, and specially instrumented research aircraft. In addition, during the 30-h period that we studied, seven RAOB's, including four special launches, were available; the 1100 and 2300 GMT soundings are shown in Fig. 10. Fig. 11 shows a 30-h time series of derived and directly measured quantities during this event. In contrast to the cold front case (Section VI), no large trends were present in P_s or the derived quantities. Note, however, the large short-term variances

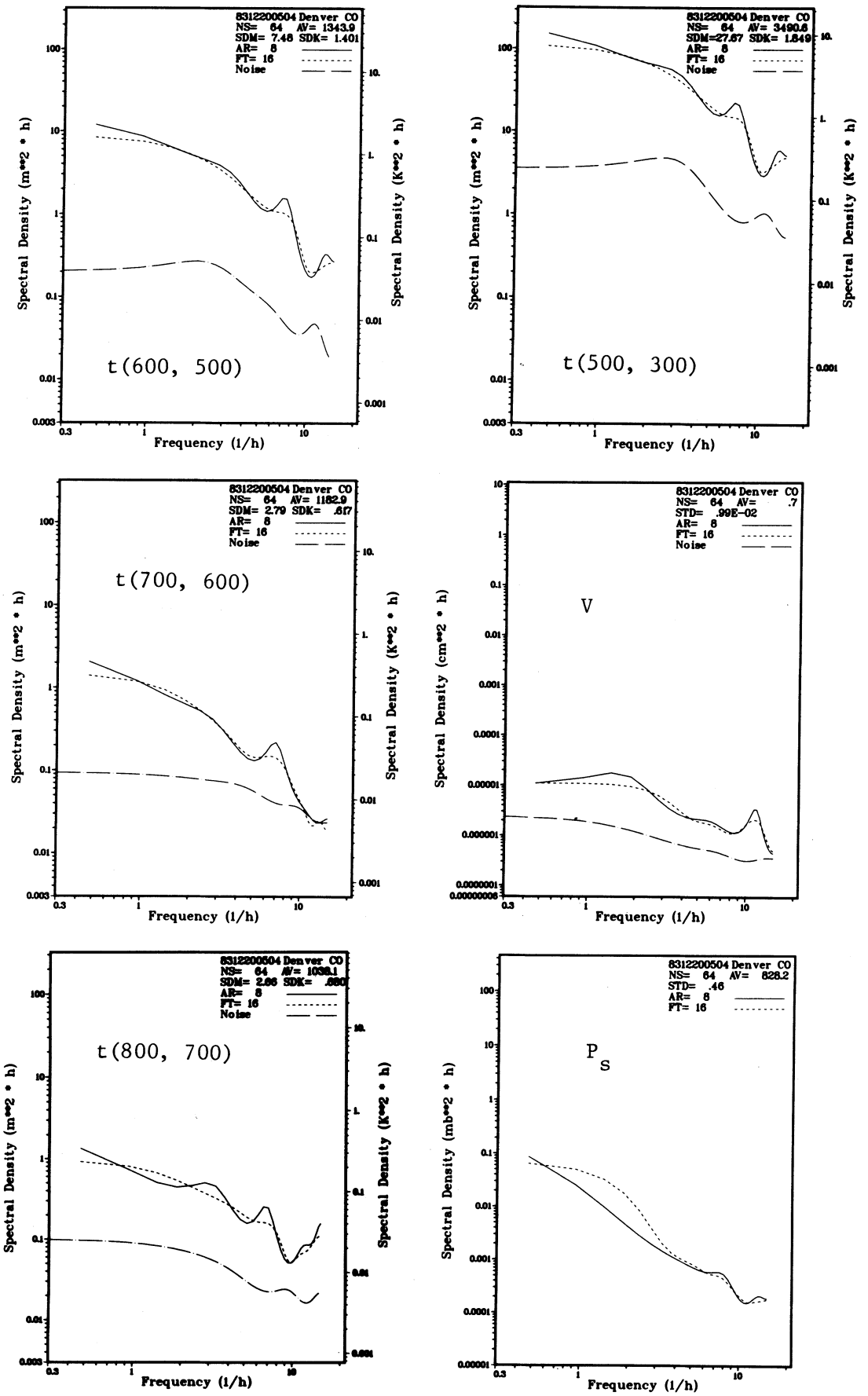

Fig. 8. Cold front, December 20, 1983, 0358-0504 GMT: Spectral density of geopotential thicknesses, precipitable water vapor, and surface pressure. Record length is 128 min; $NS = 64$; $AR = 8$; $FT = 16$.

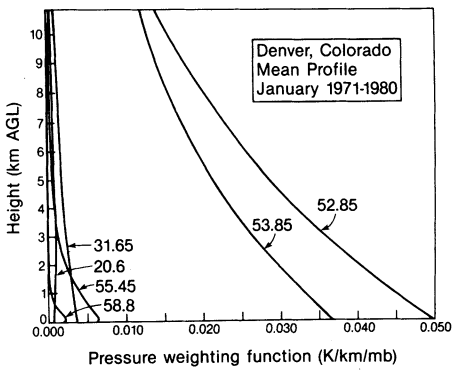

Fig. 9. Pressure weighting functions for the six-channel radiometric profiler. Calculated for Denver, CO, average profile for January 1971–1980.

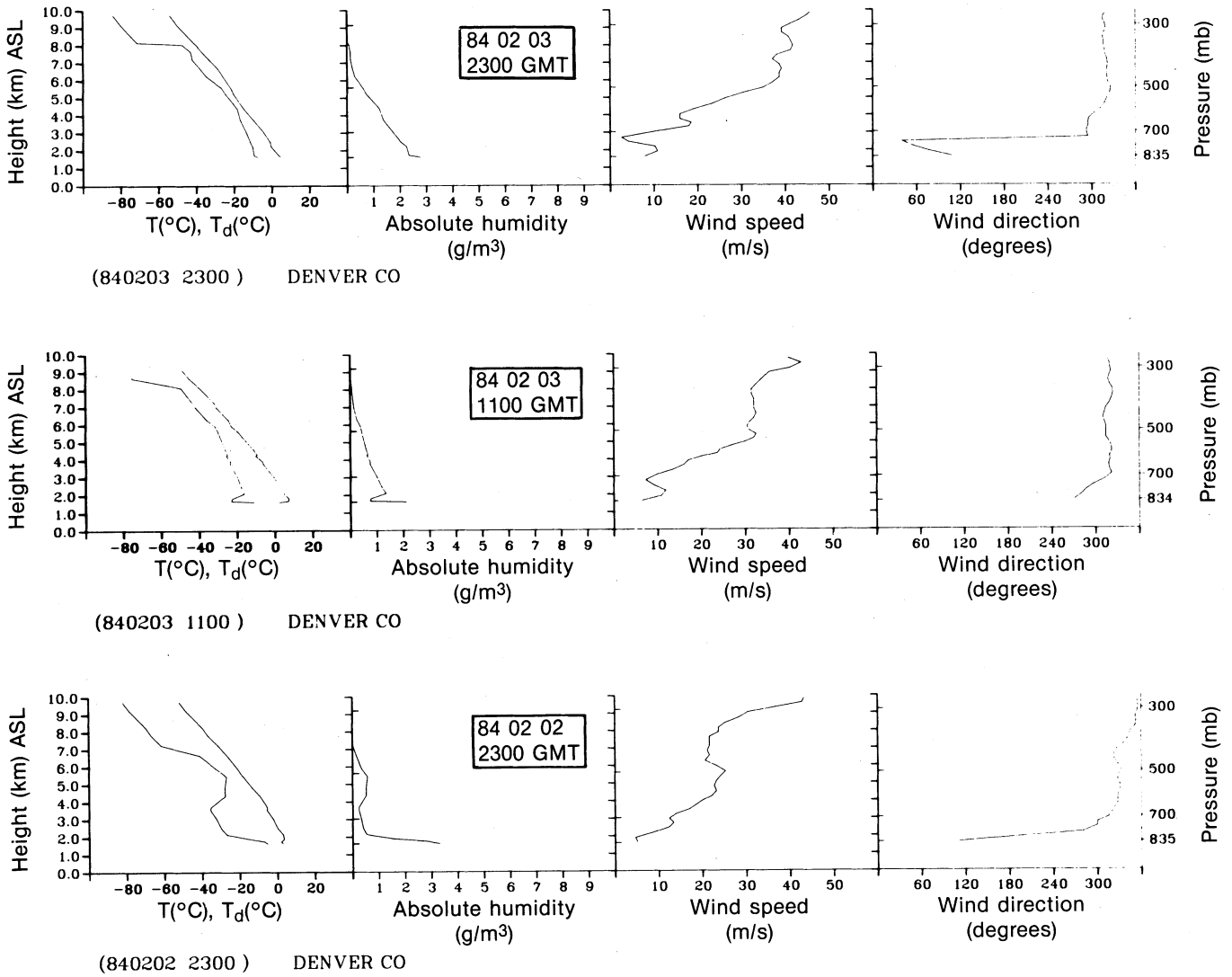

Fig. 10. Gravity wave event, February 2–4, 1984: NWS RAOB's.

occurring in the upper altitude heights and thicknesses during the 12-h period from 0000 to 1200 GMT on February 3. We analyzed a 128-min segment of data during the peak of these variations. Spectra of V, t(800 mbar, 700 mbar), t(500 mbar, 300 mbar), and P_s are shown in Fig. 12. Several clear peaks show up in the spectra; again, a FT spectral bandwidth of 3.48 cycles/h is associated with these peaks. The comparison of the radiometrically derived peaks with those observed independently is given in Table IV. As is evident from this table, the agreement between the radiometer and other information is excellent.

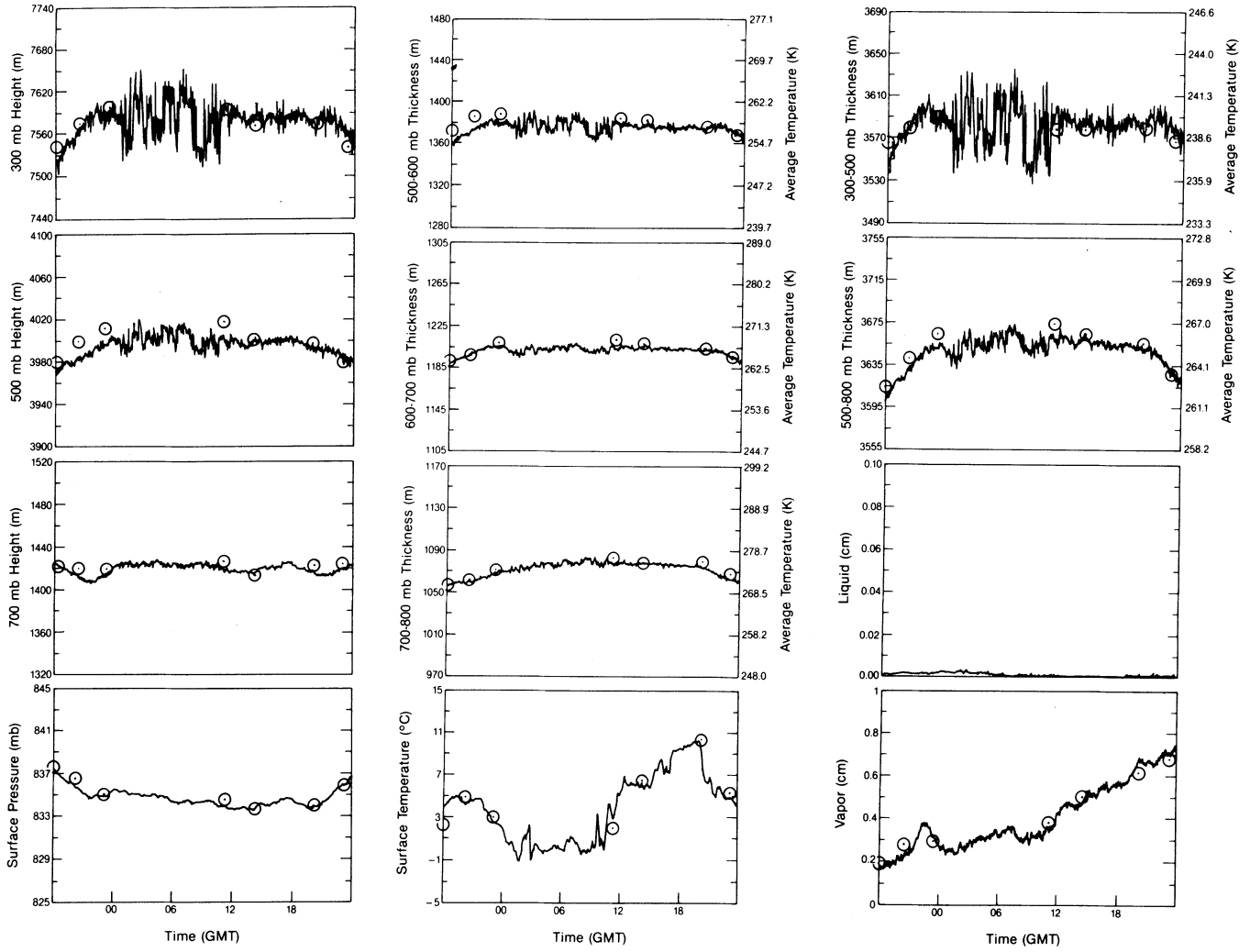

Fig. 11. Gravity wave event, February 2, 1984, 1802 GMT to February 4, 1984, 0000 GMT: 30-h time series of directly measured and derived meteorological parameters. Circled quantities refer to RAOB measurements.

TABLE IV
COMPARISON OF SPECTRAL PEAKS DERIVED BY RADIOMETER WITH THOSE DERIVED BY OTHER SOURCES OF INFORMATION FOR THE GRAVITY WAVE EVENT OF FEBRUARY 3, 1984, 0834-1040 GMT

Radiometer (cycles/h)	Surface pressure array or Satellite cloud motion (cycles/h)
13.1 ± 1.74	12.5
10.0 ± 1.74	9.4
6.5 ± 1.74	6.6

VIII. DISCUSSION

The three cases presented illustrate how rapid variations in meteorological variables can be studied using ground-based radiometers. These radiometers provide temporal continuity not hitherto available. The performance of the radiometer, both in observing a blackbody target and during an unusually calm pressure event, shows that its sensitivity to changes in geopotential height and thickness and to integrated water vapor is very high. Consequently, the combination of high temporal resolution and high sensitivity allows unique monitoring of rapidly changing events, such as frontal passages and gravity wave events.

Ground truth for the radiometrically derived quantities was available from NWS RAOB's. RAOB's are usually launched 1 h before 0000 and 1200 GMT, and, at the surface pressures commonly encountered in Denver, Colorado, take approximately 30 min to reach the 300-mbar level. During high winds, balloons can drift several kilometers, making comparisons with zenith measurements difficult. Nevertheless, the agreement of the radiometrically derived quantities with the RAOB's is generally within the predicted accuracy of the radiometer.

In the case of the cold front, the RAOB-measured precipitable vapor V was lower than the radiometrically inferred V by about 1 mm. This discrepancy can arise principally from three causes: 1) radiometric absolute calibration uncertainties of about 0.5 K at 20.6 and 31.65

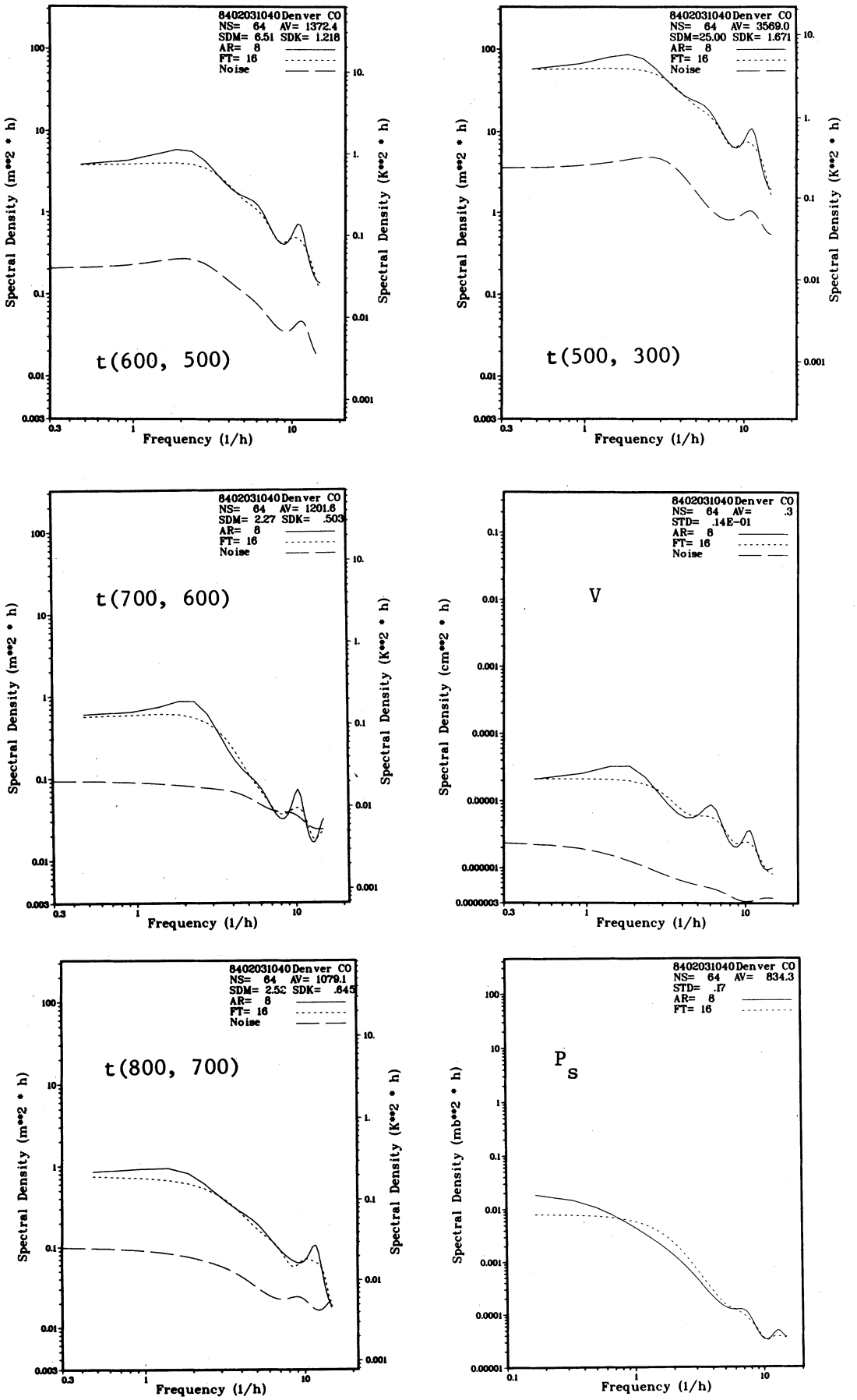

Fig. 12. Gravity wave event, February 3, 1984, 0834–1040 GMT: spectral density of geopotential thicknesses, precipitable water vapor, and surface pressure. Record length is 128 min; $NS = 64$; $AR = 8$; $FT = 16$.

GHz lead to uncertainties of about 1 mm in V; 2) the calculated water vapor absorption coefficients are too small by about 5 percent; and 3) the RAOB's measure too low a humidity under such cold conditions. None of these three causes can be summarily eliminated, since they are each approaching their current uncertainties. However, the "errors" are not important for geopotential height, since, for example, the 1 mm "error" in V, if caused by T_b calibration errors at 20.6 and 31.65 GHz, leads to an absolute $h(P)$ error of 0.3 m at 500 mbar; i.e., about 2 percent of the total difference.

Currently, meteorological information is derived from radiometric data by mathematical retrieval algorithms that ignore spectral content of these data. Perhaps, measurements of the location of spectral peaks, their amplitudes, and their relative phases between the radiometric channels could contribute significant information to the retrieval process. For example, dynamical models exist that relate spectral peaks to the mean properties of wind and temperature [3]. The coupling of models and measurements can only enhance the already useful radiometrically derived information.

Acknowledgment

The authors thank Dr. D. C. Hogg for discussing many of the aspects of this work with us. In addition, R. J. Zamora and Dr. C. G. Little, Dr. J. C. Kaimal, Dr. K. S. Gage, and Dr. R. M. Hardesty contributed many useful comments on the manuscript. M. J. Falls developed the software for displaying the RAOB data. A. J. Bedard acknowledges the encouragement of B. Colamosca of the Federal Aviation Administrative Technical Center. J. Schroeder developed the pressure weighting function plot for Fig. 9. Finally, the authors thank three anonymous reviewers whose comments added substantially to the manuscript.

References

[1] P. Ciotti, D. Solimini, and P. Basili, "Spectra of atmospheric variables as deduced from ground-based radiometry," *IEEE Trans. Geosci. Electron.*, vol. GE-17, no. 3, pp. 68–77, 1979.

[2] M. El-Raey, "Remote sensing of atmospheric waves in O_2 and H_2O microwave emissions," *Radio Sci.*, vol. 17, no. 4, pp. 766–772, 1982.

[3] M. T. Decker, F. Einaudi, and J. J. Finnigan, "The influence of gravity waves on radiometric measurements: A case study," *J. Appl. Meteor.*, vol. 20, no. 10, pp. 1231–1238, 1981.

[4] F. O. Guiraud, J. Howard, and D. C. Hogg, "A dual-channel microwave radiometer for measurement of precipitable water vapor and liquid," *IEEE Trans. Geosci. Electron.*, vol. GE-17, no. 4, pp. 129–136, 1979.

[5] D. C. Hogg, F. O. Guiraud, J. B. Snider, M. T. Decker, and E. R. Westwater, "A steerable dual-channel microwave radiometer for measurement of water vapor and liquid in the atmosphere," *J. Climate Appl. Meteor.*, vol. 22, no. 5, pp. 789–806, 1983.

[6] D. C. Hogg, F. O. Guiraud, and W. B. Sweezy, "The short-term temporal spectrum of precipitable water vapor," *Science*, vol. 213, no. 4512, pp. 1112–1113, 1981.

[7] D. C. Hogg, M. T. Decker, F. O. Guiraud, K. B. Earnshaw, D. A. Merritt, K. P. Moran, W. B. Sweezy, R. G. Strauch, E. R. Westwater, and C. G. Little, "An automatic profiler of the temperature, wind, and humidity in the troposphere," *J. Climate Appl. Meteor.*, vol. 22, no. 5, pp. 807–831, 1983.

[8] E. R. Westwater, Wang Zhenhui, N. C. Grody, and L. M. McMillin, "Remote sensing of temperature profiles from a combination of observations from the satellite-based Microwave Sounding Unit and the ground-based Profiler," *J. Atmos. Ocean. Tech.*, vol. 2, no. 2, pp. 97–109, 1985.

[9] M. T. Decker, E. R. Westwater, and F. O. Guiraud, "Experimental evaluation of ground-based microwave radiometric sensing of atmospheric temperature and water vapor profiles," *J. Appl. Meteor.*, vol. 17, no. 12, pp. 1788–1795, 1978.

[10] G. M. Jenkins and D. G. Watts, *Spectral Analysis and Its Applications*. San Francisco: Holden-Day, 1969.

[11] M. B. Priestly, *Spectral Analysis and Time Series*. London: Academic, 1981.

[12] E. R. Westwater, W. B. Sweezy, L. M. McMillin, and C. Dean, "Determination of atmospheric temperature profiles from a statistical combination of ground-based profiler and operational NOAA 6/7 satellite retrievals," *J. Climate Appl. Meteor.*, vol. 23, no. 5, pp. 689–703, 1984.

[13] W. Hoehne, "Precision of National Weather Service upper air measurements, NOAA Tech. Memo. NWS T&ED-16 (NTIS PB81-108136), 1980.

[14] M. T. Decker, "Observation of low-level frontal passages with microwave radiometers," in *Analysis of Some Cloud and Frontal Events [Recorded During the Boulder Upslope Cloud Observation Experiment (BUCOE) of 1982]*, E. E. Gossard, Ed., BUCOE Rep. 2, NOAA/ERL, Boulder, CO, pp. 27–32, 1984.

[15] E. R. Westwater, "Ground-based determination of low altitude temperature profiles by microwaves," *Mon. Wea. Rev.*, vol. 10, no. 1, pp. 15–28, 1972.

*

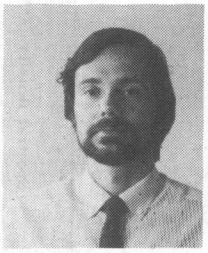

Piero Ciotti was born in Rome, Italy, on November 10, 1952. He received the Laurea (Doctor's) degree in electrical engineering (*cum laude*) from the University of Rome in 1977.

He joined the Department of Electronics of the University of Rome in 1977, where he is an Associate Professor. In 1984–1985, he conducted research at the NOAA/ERL Wave Propagation Laboratory, Boulder, CO, on a NATO-CNR fellowship. His research activity has been concerned with radiometric remote sensing of the atmosphere, microwave line-of-sight propagation, inverse electromagnetic problems, and digital-signal processing.

*

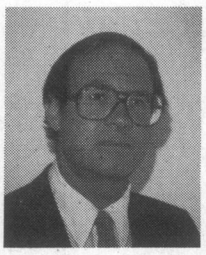

Ed R. Westwater was born on October 29, 1937, in Denver, CO. He received the B.A. degree in physics and mathematics from Western State College of Colorado in 1959, the M.S. degree in physics in 1962, and the Ph.D. degree in physics in 1970 from the University of Colorado.

He is employed as a Supervisory Physicist by the Environmental Research Laboratories of the National Oceanic and Atmospheric Administration, Boulder, CO. He currently serves as Acting Chief of the Thermodynamic Profiling Program Area in the Wave Propagation Laboratory. Since joining the Boulder Laboratories of the U.S. Department of Commerce in 1960, his research has been concerned with microwave absorption in the atmosphere, microwave and infrared radiative transfer, ground- and satellite-based remote sensing by passive radiometry, and in the application of mathematical inversion techniques to problems in remote sensing. He has taught several short courses on inversion techniques and in radiometric remote sensing of the atmosphere.

Dr. Westwater is a member of the American Meteorological Society, the Mathematical Association of America, the Society for Industrial and Applied Mathematics, the American Association for Advancement of Science, Commission F of the International Union of Radio Science, and the Commission on Radio Frequencies of the National Research Council.

Martin T. Decker (A'52–M'57) received the B.Sc. degree in electrical engineering from the University of Nebraska in 1950.

He is currently employed by the Cooperative Institute for Research in Environmental Sciences of the University of Colorado/NOAA in Boulder. From 1950 to 1984, he was employed by the Boulder Laboratories of the U.S. Department of Commerce, including the National Bureau of Standards and the NOAA Environmental Research Laboratories. His research has been in the areas of radio propagation and remote sensing of the atmosphere. Remote sensing studies have included the development and evaluation of microwave radiometric techniques for the ground-based sensing of atmospheric temperature, vapor, liquid, and related properties.

Mr. Decker is a member of the American Meteorological Society, Commission F of the International Union of Radio Science, and Sigma Xi.

*

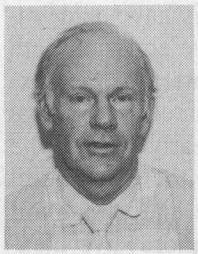

J. Alfred Bedard, Jr. was born on November 29, 1935 in Brooklyn, NY. He received the B.S. degree in physics from Boston College in 1957 and the M.S. and Ph.D. degrees in aerospace engineering sciences, both from the University of Colorado, in 1976 and 1982, respectively.

He is currently employed as a Supervisory Research Scientist by the Environmental Research Laboratories of NOAA, Boulder, CO. He has worked in the Department of Commerce Laboratories since 1960 on topics ranging from atmospheric acoustics to methods for the detection of airport windshear. He is an Associate Professor Adjoint at the University of Colorado.

Dr. Bedard is a member of the American Meteorological Society, the Acoustical Society of America, and the American Institute of Aeronautics and Astronautics.

*

B. Boba Stankov received the B.S. degree in meteorology in 1964 from the University of Belgrade, Yugoslavia, and the M.S. degree in atmospheric sciences from Colorado State University, Fort Collins, in 1971. She completed the requirements for the Ph.D. degree in astrogeophysics at the University of Colorado, Boulder, in 1978.

She spent eight years at the National Center for Atmospheric Research in Boulder, concentrating on observational research of the atmospheric boundary layer using aircraft data. Currently, she is with the Wave Propagation Laboratory at NOAA in Boulder. She is using the data from the radiometric and the wind profiling systems to study mesoscale meteorological phenomena.